3D Sparse Finite-Difference Time-Domain Simulation of Silicon Photonic Integrated Circuits

C. Doerr
Acacia Communications, 1301 Route 36, Hazlet, NJ 07730, USA
chris.doerr@acacia-inc.com

Abstract: Silicon photonic circuits are growing in size yet designing them often requires full-vectorial 3D simulation. Simulation times can be impractical with today's tools. We propose a new simulation tool that is significantly faster.

OCIS codes: (060.2330) Fiber optics communications (130.3120) Integrated optics devices.

1. Introduction

In a silicon photonic integrated circuit (PIC), the light is guided in silicon surrounded on all sides by glass. This high index contrast in two dimensions allows for extremely compact optical elements, tight bends, excellent polarization handling properties, and fast modulators [1]. However, silicon PICs generally require 3D full-vectorial simulations for accuracy. Such simulations are highly time and memory intensive. So much so that 3D simulation of any intricate PIC portion larger than a few 100 μm^2 is impractical with personal computers. There are two main 3D full-vectorial simulation methods widely used today: the eigenmode expansion (EME) method [2] and the finite-difference time-domain (FDTD) method [3]. EME relies on mode calculations, and while faster than FDTD, calculates for only one wavelength at a time and can have difficulties with wide structures [4]. FDTD is generally agreed to be the most accurate method and can handle any situation. However, it is also very slow and memory intensive. We propose and demonstrate a method based on FDTD that can be more than ten times faster and occupies significantly less memory for low-dispersive structures.

2. Theory

The finite-difference time-domain (FDTD) method for electromagnetic simulation was proposed by Yee [3]. In 3D FDTD, the PIC is inside a designated volume divided into a $x/y/z$ grid. The grid size must be substantially smaller than the optical wavelengths of interest. There are six electromagnetic field components at each grid point, E_x, E_y, E_z, H_x, H_y, and H_z, the electric and magnetic field strengths. The difference equations (1-2), derived directly from Maxwell's equations in the isotropic, non-magnetic-material case, are applied at each time step. Each equation is actually three equations in which the spatial indices x, y, and z are cycled through. t is time, μ_0 is the vacuum permeability, ε_0 is the vacuum permitivity, and ε_r is the permittivity at point x,y,z. FDTD is a direct simulation in that the fields are purely real, and there are no approximations except for the space and time quantization. Conventional FDTD is so slow because at each time step, the equations must be applied to all the points in the volume.

$$-\mu_0 \frac{\partial H_x}{\partial t} = \frac{\partial E_z}{\partial y} - \frac{\partial E_y}{\partial z} \tag{1}$$

$$\varepsilon_0 \varepsilon_r \frac{\partial E_x}{\partial t} = \frac{\partial H_z}{\partial y} - \frac{\partial H_y}{\partial z} \tag{2}$$

Our proposed technique is called sparse FDTD, and a 2D version was developed in [5]. Similar to sparse matrix calculations in which non-zero matrix elements are stored in a list, Maxwell's equations are applied to only the points that contain optical power above a certain level. This is done by keeping in memory only a list of the "active" points. Each entry of the list contains the six field component amplitudes and the spatial coordinate of that point. At each time step, operations are performed on the list entries, new entries are added to the list, and entries with optical power below a certain value are removed from the list. For example, suppose the simulation volume is 100 x 100 x 100 points, yet only 100 of these points contain significant optical power. Conventional FDTD applies Maxwell's equations 10^6 times every time step, whereas sparse FDTD applies them only 10^2 times every time step. The list management is done as

978-1-55752-937-4/15/$31.00 ©2015 Optical Society of America

follows: when an entry is removed from the active-point list, it leaves a hole in the list. A separate list of holes is maintained. When a new entry is to be added, one first checks if any holes are available from the hole list. If so, the new entry is added in the hole, and the hole is removed from the hole list. If not, the new entry is placed at the end of the active-point list of active points and the list length is incremented.

In conventional FDTD, at each time step, the change in value to the field at each point comes from applying Eqs. (1-2). We cannot use these equations directly with sparse FDTD because they do not easily distinguish when to add new entries to the list. Thus we rewrite the equations as shown in (3-5) and (6-8). The indices x, y, and z are cycled through and thus (3-8) represent 18 total equations. Unless otherwise noted, the point location is x, y, z. $\Delta x, \Delta y, \Delta z$ are the grid periods. Eq. (3) (which represents three equations) is straightforwardly applied to all the entries in the list. For Eq. (4), it is first determined if the list already contains an entry with coordinate $-\Delta z$ away from the entry under consideration. If it does, Eq. (4) is simply applied. If not, a new entry with coordinates $x, y, z-\Delta z$ is created and then Eq. (4) is applied to that new point. Likewise with Eq. (5). Then the same process is repeated for Eqs. (6-8).

$$H_x^{\text{new}} = H_x + \frac{\Delta t}{\mu_0}\left(\frac{E_z}{\Delta y} - \frac{E_y}{\Delta z}\right) \tag{3}$$

$$H_x^{\text{new}}|_{z-\Delta z} = H_x|_{z-\Delta z} + \frac{\Delta t}{\mu_0}\frac{E_y}{\Delta z} \tag{4}$$

$$H_x^{\text{new}}|_{y-\Delta y} = H_x|_{y-\Delta y} - \frac{\Delta t}{\mu_0}\frac{E_z}{\Delta y} \tag{5}$$

$$E_x^{\text{new}} = E_x + \frac{\Delta t}{\varepsilon_0 \varepsilon_r}\left(\frac{H_z}{\Delta y} - \frac{H_y}{\Delta z}\right) \tag{6}$$

$$E_x^{\text{new}}|_{z+\Delta z} = E_x|_{z+\Delta z} + \frac{\Delta t}{\varepsilon_0 \varepsilon_r}\frac{H_y}{\Delta z} \tag{7}$$

$$E_x^{\text{new}}|_{y+\Delta y} = E_x|_{y+\Delta y} - \frac{\Delta t}{\varepsilon_0 \varepsilon_r}\frac{H_z}{\Delta y} \tag{8}$$

3. Simulation example

The simulation starts with a pulse launched into a waveguide. The field is recorded at the beginning and end and is Fourier transformed to calculate the transmissivity vs. wavelength. Indeed, it is an advantage of FDTD, conventional or sparse, that the full wavelength response is calculated in one shot. Because PIC waveguides are dispersive, there is an optimum pulse width and chirp to launch for a given structure to achieve the shortest simulation time. If the pulse is too short, it spreads too much from the dispersion and the list becomes very long and slows down the simulation. If the pulse is too long, again the list is very long and slows down the simulation. A uniform grid is used. The dielectric constant is averaged when a boundary falls between grid points.

We simulate a polarization splitter in silicon wire waveguides. The polarization splitter is a directional coupler which couples transverse magnetic (TM) polarization but not transverse electric (TE) polarization due the large effective index difference between TE and TM [6]. The waveguide layout is shown in Fig. 1 (a). The waveguide height is 220 nm and width is 430 nm. The coupler gap is 0.40 μm and length is 10.4 μm. A pulse is launched in either the quasi-TE or TM modes and allowed to propagate to the end of the structure. The TE launch is a 6-ps, 0.02-chirp pulse, and the TM launch is a chirped 25-ps, 0.16 chirp pulse. The TM pulse had to be significantly longer and more chirped because the quasi-TM exhibits high group velocity dispersion in silicon wire waveguides. The center wavelength is 1546 nm. The grid sizes are 45, 45, 30 nm for x, y, and z, respectively. The power discard threshold was 10^4 times lower than the maximum power at a given moment.

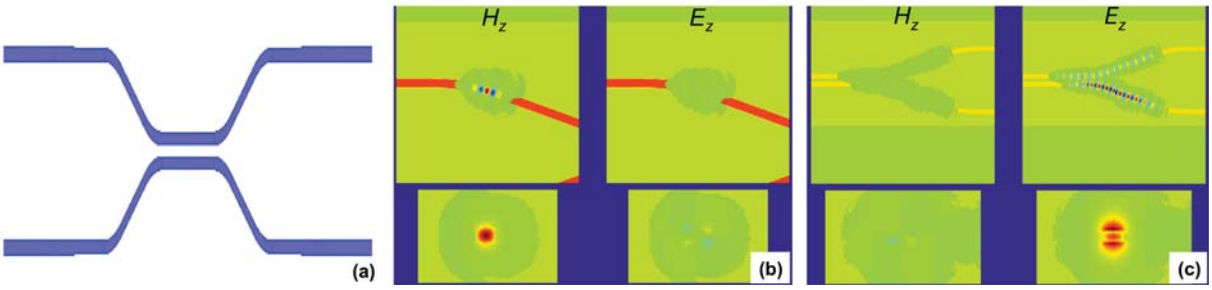

Fig. 1. (a) Waveguide layout for the polarization splitter, stretched vertically. Total length is 74 μm. (b) and (c) screen shots during simulation for TE- and TM-polarized launch, respectively.

Screen shots taken during simulation are shown in Figs. 1 (b) and (c). The left column shows the H_z field from top

and cross-section views, and likewise the E_z field in the right column. Thus the left and right columns indicate the quasi-TE and TM modes, respectively. The active points are colored. The light green area indicates the extent of the active points. The 3D active volume has a caterpillar shape. When the field splits in the coupler into two branches, two caterpillar shapes are created.

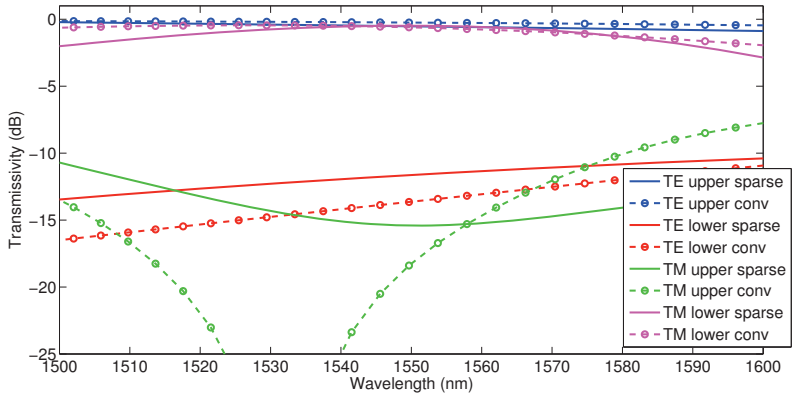

Fig. 2. Calculated transmissivities for quasi-TE and -TM polarization launch into the polarization splitter for sparse and conventional FDTD.

The quasi-TE and -TM calculations took 16 and 117 minutes, respectively, on a personal computer. The TM calculation takes so much longer because the mode is larger and the pulse is longer, making it ∼10 times longer to simulate than TE. The calculated transmissivities from the upper left port to the two right ports are shown in Fig. 2.

We compared this result to that of a commercial conventional FDTD simulator, Lumerical [7]. Lumerical used a variable grid ranging from 30 to 70 nm. In the future, sparse FDTD could also use a variable grid to speed execution. Lumerical took ∼340 minutes to complete for each polarization, which is 21 and 3 times slower for TE and TM, respectively, than sparse FDTD. As one can see from Fig. 2, sparse FDTD has good agreement with Lumerical for all cases except for TM in the upper output port at wavelengths off the center wavelength. This inaccuracy is likely coming from the fact that sparse FDTD discards points with low power, and thus for ports with low total power, such as the upper output port for TM, too many points may be discarded. One remedy is to increase the discarding threshold, at the expense of more simulation time.

In conclusion, a new 3D full-vectorial simulation technique was demonstrated. It can significantly reduce the simulation time of silicon PICs, by more than an order of magnitude for structures with low dispersion. The author thanks Long Chen and Diedrik Vermeulen for helpful discussions.

References

1. R. Soref, “The Past, Present, and Future of Silicon Photonics,” *IEEE J. Sel. Topics Quantum Electron.*, vol. 12, no. 6, pp. 1678–1687, 2006.
2. P. Bienstman and R. Baets, “Optical modelling of photonic crystals and VCSELs using eigenmode expansion and perfectly matched layers,” *Opt. and Quant. Electron.*, vol. 33, pp. 327–341, 2001.
3. K. S. Yee, “Numerical Solution of Initial Boundary Value Problems Involving Maxwell’s Equations in Isotropic Media,” *Antennas and Propagation, IEEE Transactions on*, 1966.
4. D. F. G. Gallagher and T. P. Felici, “Eigenmode Expansion Methods for Photonics - Pros and Cons,” in *SPIE Proceedings*, 2003, pp. 1–14.
5. C. R. Doerr, “Sparse Finite Difference Time Domain Method,” *IEEE Photonics Technology Letters*, vol. 25, no. 23, pp. 2259–2262, Dec. 2013.
6. H. Fukuda, K. Yamada, T. Tsuchizawa, T. Watanabe, H. Shinojima, and S.-I. Itabashi, “Silicon photonic circuit with polarization diversity.” *Optics express*, vol. 16, no. 7, pp. 4872–80, Mar. 2008.
7. J. Pond, C. Cone, L. Chrostowski, J. Klein, J. Flueckiger, A. Liu, D. McGuire, and X. Wang, “A complete design flow for silicon photonics,” p. 913310, May 2014.